







# Vibrational properties of CdGa<sub>2</sub>S<sub>4</sub> at high pressure

Cite as: J. Appl. Phys. **125**, 115901 (2019); <https://doi.org/10.1063/1.5080503>

Submitted: 09 November 2018 . Accepted: 28 February 2019 . Published Online: 19 March 2019

S. Gallego-Parra , O. Gomis , R. Vilaplana , H. M. Ortiz, E. Pérez-González, R. Luna, P. Rodríguez-Hernández , A. Muñoz , V. V. Ursaki, I. M. Tiginyanu, and F. J. Manjón 



View Online



Export Citation



CrossMark

Applied Physics Reviews  
Now accepting original research

2017 Journal  
Impact Factor:  
**12.894**

AIP  
Publishing

# Vibrational properties of CdGa<sub>2</sub>S<sub>4</sub> at high pressure

Cite as: J. Appl. Phys. **125**, 115901 (2019); doi: 10.1063/1.5080503

Submitted: 9 November 2018 · Accepted: 28 February 2019 ·

Published Online: 19 March 2019



S. Gallego-Parra,<sup>1</sup> O. Gomis,<sup>2,a)</sup> R. Vilaplana,<sup>2</sup> H. M. Ortiz,<sup>1,3,4</sup> E. Pérez-González,<sup>5</sup> R. Luna,<sup>2</sup>  
P. Rodríguez-Hernández,<sup>5</sup> A. Muñoz,<sup>5</sup> V. V. Ursaki,<sup>6</sup> I. M. Tiginyanu,<sup>7</sup> and F. J. Manjón<sup>1</sup>

## AFFILIATIONS

<sup>1</sup>Instituto de Diseño para la Fabricación y Producción Automatizada, MALTA Consolider Team, Universitat Politècnica de València, 46022 València, Spain

<sup>2</sup>Centro de Tecnologías Físicas: Acústica, Materiales y Astrofísica, MALTA Consolider Team, Universitat Politècnica de València, 46022 València, Spain

<sup>3</sup>CINVESTAV-Departamento de Nanociencia y Nanotecnología, Unidad Querétaro, 76230 Querétaro, México

<sup>4</sup>Proyecto Curricular Licenciatura en Física, Universidad Distrital "Fco. Jose de Caldas", Bogotá, Colombia

<sup>5</sup>Departamento de Física, Instituto de Materiales y Nanotecnología, MALTA Consolider Team, Universidad de La Laguna, 38205 Tenerife, Spain

<sup>6</sup>Ghitu Institute of Electronic Engineering and Nanotechnologies, 2028 Chisinau, Moldova

<sup>7</sup>National Center for Materials Study and Testing, Technical University of Moldova, 2004 Chisinau, Moldova

<sup>a)</sup>Author to whom correspondence should be addressed: [osgoi@fis.upv.es](mailto:osgoi@fis.upv.es)

## ABSTRACT

Raman scattering measurements have been performed in cadmium digallium sulphide (CdGa<sub>2</sub>S<sub>4</sub>) with defect chalcopyrite structure up to 25 GPa in order to study its pressure-induced phase transitions. These measurements have been complemented and compared with lattice-dynamics *ab initio* calculations including the TO-LO splitting at high pressures in order to provide a better assignment of experimental Raman modes. In addition, experimental and theoretical Grüneisen parameters have been reported in order to calculate the molar heat capacity and thermal expansion coefficient of CdGa<sub>2</sub>S<sub>4</sub>. Our measurements provide evidence that CdGa<sub>2</sub>S<sub>4</sub> undergoes an irreversible phase transition above 15 GPa to a Raman-inactive phase, likely with a disordered rock salt structure. Moreover, the Raman spectrum observed on downstroke from 25 GPa to 2 GPa has been attributed to a new phase, tentatively identified as a disordered zinc blende structure, that undergoes a reversible phase transition to the Raman-inactive phase above 10 GPa.

Published under license by AIP Publishing. <https://doi.org/10.1063/1.5080503>

## I. INTRODUCTION

$A^{II}B_2^{III}X_4^{VI}$  compounds are distorted tetrahedrally-coordinated compounds characterized by the presence of stoichiometric vacancies in the unit cell. Vacancies are needed to obey the Grimm-Sommerfeld rule and maintain the charge neutrality, as in other tetrahedrally-coordinated structures derived from the diamond structure.<sup>1</sup>  $A^{II}B_2^{III}X_4^{VI}$  compounds are also known as ordered-vacancy compounds (OVCs) and they represent a clear intermediate stage between perfect crystals and amorphous materials. In particular, CdGa<sub>2</sub>S<sub>4</sub> crystallizes in the defect chalcopyrite (DC) structure [space group (s.g.)  $I\bar{4}$ , No. 82,  $Z=2$ ]. Its unit cell can be visualized by doubling the zinc blende (ZB) one (s.g.  $F\bar{4}3m$ , No. 216,  $Z=4$ ) of an AX compound along the *c*-axis and replacing four equal cations of the ZB structure by one Cd cation, two Ga cations, and one vacancy [Fig. 1(a)].

The presence of vacancies in OVCs yields relevant properties in comparison with their homologue AX, BX, and ABX<sub>2</sub> compounds, like higher compressibilities,<sup>2-4</sup> good performance as host materials<sup>5,6</sup> and suitable valence electron concentration, large second harmonic generation, and extensive damage threshold for mid-IR nonlinear optics.<sup>7,8</sup> The most remarkable fields of application of OVCs, due to their wide bandgap, high photosensitivity, bright photoluminescence, and long-term stability of many parameters are photovoltaic cells,<sup>9</sup> optoelectronic devices,<sup>10</sup> temperature sensors,<sup>11</sup> and optical filters.<sup>12,13</sup> In particular, CdGa<sub>2</sub>S<sub>4</sub> has raised considerable attention in the field of nonlinear optics.<sup>12-14</sup>

Several high-pressure (HP) studies of the properties of OVCs have been reported in the last few years. A combination of multiple experimental techniques such as X-ray diffraction (XRD), Raman

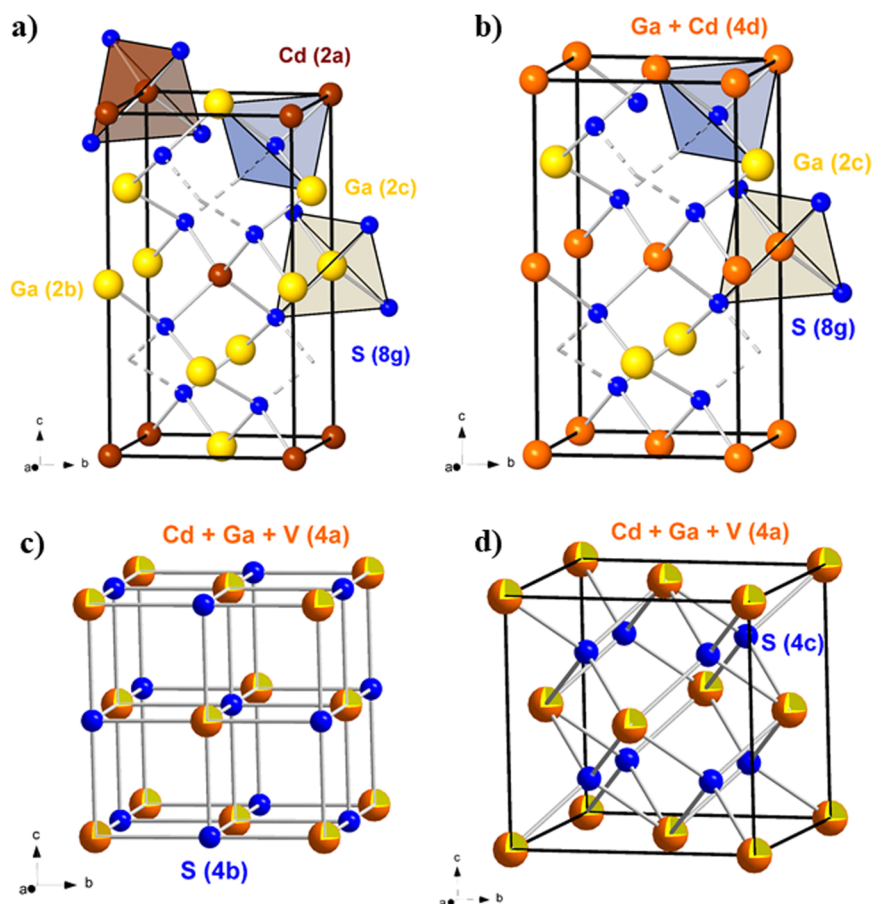


**FIG. 1.** Crystalline structure of (a) DC- $\text{CdGa}_2\text{S}_4$ , (b) DS- $\text{CdGa}_2\text{S}_4$ , (c) DR- $\text{CdGa}_2\text{S}_4$ , and (d) DZ- $\text{CdGa}_2\text{S}_4$ . Medium brown balls are Cd cations, big yellow balls are Ga cations, and small blue balls are S anions. Orange and open orange balls represent the sites shared between Cd + Ga and Cd + Ga + V (vacancy), respectively. The Wyckoff sites are given in parenthesis for the phases described.

scattering (RS), optical reflectivity, and/or absorption measurements at HP have proven to be a successful way to outline pressure-induced phase transitions (PTs).<sup>15–19</sup> Many OVCs have been found to exhibit a pressure-induced order-disorder PT from a DC or a defect stannite (DS) structure (s.g.  $I\bar{4}2m$ , No. 121,  $Z = 2$ ) [Fig. 1(b)] to a disordered rock salt (DR) structure (s.g.  $Fm\bar{3}m$ , No. 225,  $Z = 1$ ) [Fig. 1(c)]. In the DR structure,  $A^{\text{II}}$  and  $B^{\text{III}}$  cations and vacancies are fully mixed in  $4a$  Wyckoff sites, while  $4b$  sites are fully occupied by anions. Before reaching the DR structure, other defect or disordered structures might occur at intermediate pressures. For instance, DC- $\text{CdGa}_2\text{Se}_4$  and DC- $\text{HgGa}_2\text{S}_4$  were found to transform first to the DS phase at 18 GPa before undergoing the DR phase above 20 and 23 GPa, respectively.<sup>20,21</sup>

Earlier HP studies have focused on the properties of  $\text{CdGa}_2\text{S}_4$ . HP-XRD measurements of Errandonea *et al.* showed a pressure-induced DC-to-DR transition above 17 GPa with a volume collapse of ca. 5% that evidenced the first-order nature of this pressure-induced PT.<sup>22</sup> On the other hand, Aliabad *et al.* studied the structural, electronic, optical, and thermoelectric properties of  $\text{CdGa}_2\text{S}_4$  at HP by density functional theory (DFT) calculations.<sup>23,24</sup> They concluded that  $\text{CdGa}_2\text{S}_4$  is an interesting p-type thermoelectric material with the best figure of merit (1.04) achieved at 0.58 GPa along the  $z$ -direction at 800 K. Additionally, Shikimaka *et al.* recently

investigated experimentally the mechanical properties of  $\text{CdGa}_2\text{S}_4$  and  $\text{CdGa}_2\text{Se}_4$  crystals under indentation and used RS measurements to study the possible indentation-induced PTs.<sup>25</sup> They found that a disordered zinc blende (DZ) phase (s.g.  $F\bar{4}3m$ , No. 216,  $Z = 4$ ) [Fig. 1(d)] was present in recovered samples indented with high loads. This suggests that the DC-to-DR PT in adamantite-type OVCs can be induced by indentation at much smaller pressures than by hydrostatic compression. This is due to the combination of hydrostatic and shear stresses in the indentation process, thus opening a door for the synthesis of new phases with interesting properties for technological applications.

HP-RS measurements in  $\text{CdGa}_2\text{S}_4$  were also performed by Ursaki *et al.*<sup>26</sup> and Mitani *et al.*,<sup>27</sup> who observed the disappearance of Raman peaks around 15 GPa; a fact that is consistent with the DR phase found by HP-XRD above 17 GPa.<sup>22</sup> However, these two HP-RS works could only tentatively identify the LO counterparts of the Raman modes and showed slight differences in the behavior of the Raman modes at HP. The main discrepancies between the two works were (1) quite different pressure coefficients were assigned to Raman modes of the low-frequency region, (2) the pressure-induced DC-to-DR PT was considered to be irreversible by Ursaki *et al.*<sup>26</sup> and reversible by Mitani *et al.*,<sup>27</sup> and (3) both works discussed the presence of two order-disorder stages prior to the DC-to-DR PT, but gave considerably different pressures for the onset of those two

stages. Parallel to these experimental HP-RS studies focused on  $\text{CdGa}_2\text{S}_4$ , Fuentes-Cabrera reported lattice dynamics *ab initio* calculations at the Brillouin zone (BZ) center.<sup>28</sup> The good agreement of his simulations, which did not include any disorder effect, with the results of Ursaki *et al.* led Fuentes-Cabrera to hesitate about the order-disorder stages previously proposed. Unfortunately, those *ab initio* calculations did not report LO-TO splitting of Raman modes, characteristic of acentric  $\text{DC-CdGa}_2\text{S}_4$  and other OVCs, so a complete discussion of the assignment of the LO modes and of the order-disorder stages in  $\text{DC-CdGa}_2\text{S}_4$  based on a comparison of experimental and theoretical frequencies and their pressure coefficients could not be fully accomplished. In summary, the different results commented upon here clearly suggest that additional HP experimental and theoretical studies on  $\text{CdGa}_2\text{S}_4$  are required to shed light on these unresolved questions.

In this work, we report HP-RS measurements in  $\text{DC-CdGa}_2\text{S}_4$  up to 25 GPa in order to study the pressure-induced DC-to-DR PT and determine the reversibility or irreversibility of such PT and the possible order-disorder stages prior to that PT. Moreover, the measurements have been complemented and compared with lattice-dynamics *ab initio* calculations including the TO-LO splitting at high pressures in order to provide a better assignment of experimental Raman modes and help in the discussion of the possible order-disorder stages. Finally, we report the experimental and theoretical Grüneisen parameters of  $\text{CdGa}_2\text{S}_4$  in order to calculate its thermodynamic properties, like the molar heat capacity and the thermal expansion coefficient.

## II. EXPERIMENTAL SECTION

Single crystals of  $\text{DC-CdGa}_2\text{S}_4$  were grown from its constituents CdS and  $\text{Ga}_2\text{S}_3$  by the chemical vapor transport method using iodine as a transport agent.<sup>26</sup> The as-grown crystals represent triangular prisms with mirror surfaces. Chemical and structural analyses have shown the stoichiometric composition of the crystals with no spurious phases. The comparison of our RS measurements at room pressure with the available literature gives further evidence for the purity of our samples.

Non-resonant unpolarized HP-RS measurements at room temperature were performed with a LabRAM HR UV microspectrometer coupled to a Peltier-cooled CCD camera. We used a 532.12 nm (2.33 eV) laser excitation line with a power of 10 mW and a spectral resolution better than  $2\text{ cm}^{-1}$ . In order to analyze the Raman spectra under pressure, Raman peaks have been fitted when possible to a Voigt profile (Lorentzian profile convoluted by a Gaussian due to the limited resolution of the spectrometer) where the spectrometer resolution is a fixed parameter. For HP-RS experiments, samples loaded in a diamond anvil cell were surrounded by a 16:3:1 methanol-ethanol-water mixture acting as a pressure-transmitting medium, which provides a reasonable quasi-hydrostatic behavior in the pressure range studied.<sup>29</sup> Ruby balls evenly distributed in the pressure chamber were used to measure the pressure by the ruby fluorescence method.<sup>30,31</sup> The shape and separation of the  $R_1$  and  $R_2$  ruby lines were checked at each pressure and neither a significant increase in width nor an overlapping of both peaks were detected, thus suggesting that nearly quasi-hydrostatic conditions are fulfilled in our experiments.

## III. THEORETICAL CALCULATION DETAILS

First principles total-energy calculations were performed within the framework of the density functional theory (DFT) and the projector-augmented wave (PAW)<sup>32</sup> method using the Vienna *ab initio* simulation package (VASP).<sup>33</sup> A plane-wave energy cutoff of 520 eV was used to ensure a high precision in the calculations. We also performed simulations with the Quantum Espresso package<sup>34</sup> using ultrasoft pseudo-potentials. A cutoff energy of 60 Ry and a k-mesh of  $(4 \times 4 \times 4)$  were employed to obtain well-converged results. The exchange and correlation energy was taken with VASP and Quantum Espresso in the generalized gradient approximation (GGA) with the PBEsol prescription.<sup>35</sup> For the sake of simplicity, only the ordered DC structure was simulated.

Initially, lattice-dynamics calculations of phonon modes for the DC structure were performed at the zone center ( $\Gamma$  point) of the Brillouin zone (BZ) using VASP and the direct force-constant approach,<sup>35,36</sup> as in previous studies of OVCs where details of the lattice dynamics calculations in the DC structure can be consulted.<sup>15,16,19–21,36</sup> The frequencies of the normal modes were provided by the diagonalization of the dynamical matrix at  $\Gamma$ . These calculations also allowed to identify the symmetry and eigenvectors of the vibrational modes. In this work, we have gone one step further and have obtained the vibrational LO-TO splitting at  $\Gamma$ . For that purpose, a non-analytical term due to the long-range interaction of the electric field must be taken into account. The phonon frequencies at  $\Gamma$ , including TO and LO phonon splitting, were evaluated using Density Functional Perturbation Theory (DFPT) with the Quantum Espresso package. To check the consistency of calculations, we compared the phonon frequencies calculated with Quantum Espresso and VASP finding a good agreement for the TO modes. Therefore, in the following, we will only present theoretical results for Raman-active modes of the DC phase including the LO-TO splitting obtained with the Quantum Espresso package.

## IV. RESULTS AND DISCUSSION

### A. First upstroke

According to group theory,  $\text{DC-CdGa}_2\text{S}_4$  (with 7 atoms per primitive unit cell) exhibits 21 vibrational modes at the BZ center that are described by the following irreducible representation:

$$\Gamma = 3A(\text{R}) + 5B(\text{R}, \text{IR}) + 5E(\text{R}, \text{IR}) + B + E$$

where  $E$  modes are doubly degenerated. Two modes are acoustic (an  $E$  mode and a  $B$  mode) and the rest are optical modes. The  $A$  modes are non-polar modes, which are Raman active (R), while the  $B$  and  $E$  modes are polar modes, show LO-TO splitting, and are both Raman and infrared (IR) active. Taking into account the LO-TO splitting of the  $E$  and  $B$  modes, it should be possible to observe 23 Raman modes on  $\text{DC-CdGa}_2\text{S}_4$ . For the sake of clarity, we label each mode hereon with a letter concerning its symmetry and a superscript that numbers it. Besides, a subscript is added to  $B$  and  $E$  modes which points out whether it is the LO or TO counterpart. No subscript means that LO-TO splitting is not observed.

Figure 2 shows the Raman spectra of DC-CdGa<sub>2</sub>S<sub>4</sub> during the first upstroke up to 25 GPa. The Raman spectrum of DC-CdGa<sub>2</sub>S<sub>4</sub> can be divided into three regions: low-frequency (below 200 cm<sup>-1</sup>), medium-frequency (between 200 and 300 cm<sup>-1</sup>), and high-frequency (above 300 cm<sup>-1</sup>). The extensive literature has allowed to show that the low- and high-frequency regions are deeply dependent on the mass of A<sup>II</sup> (Cd) and B<sup>III</sup> (Ga) cations, respectively; although the high-frequency region is mainly dependent of anions since it is usually dominated by stretching modes characterized by the vibrations of anions (S) against the cations.<sup>36–39</sup>

The most intense Raman peak is the lowest-frequency A<sup>I</sup> mode, known as the breathing mode since it is related to the symmetric vibration of anions around the stoichiometric vacancies. Strong A-symmetry Raman modes have been observed in other OVCs and even in mixed crystals with the DC structure.<sup>16,20,21,36,39</sup>

The breathing mode is mainly influenced by the anion substitution and to a minor extent by the A<sup>II</sup> cation.<sup>37,38</sup> Regarding the B and E modes, their strong cation dependence, mainly in the low and high-frequency regions, has allowed to understand the different vibrations

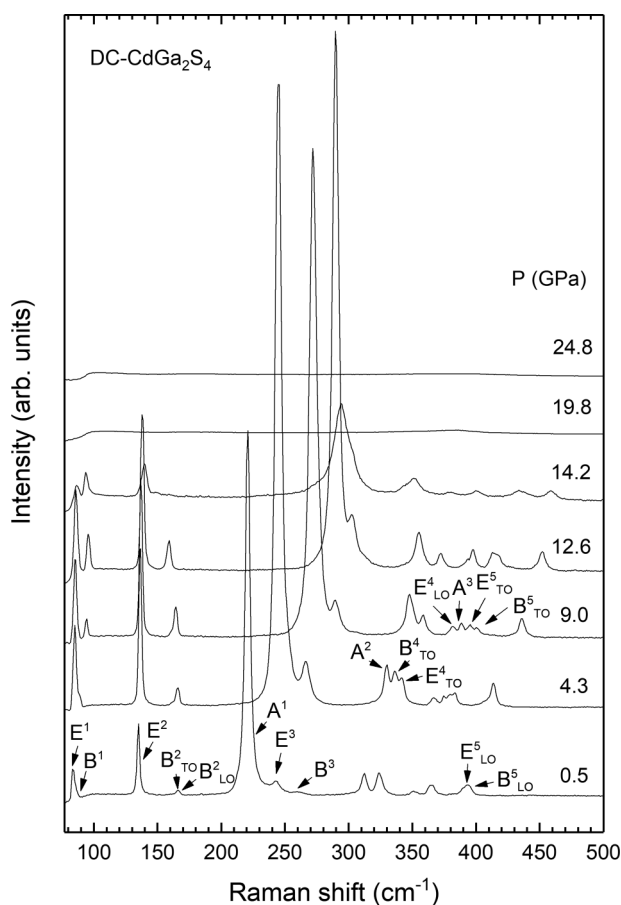


FIG. 2. Room temperature Raman scattering spectra of DC-CdGa<sub>2</sub>S<sub>4</sub> up to 24.8 GPa.

that occur inside the unit cell.<sup>40,41</sup> In fact, the substitution of A<sup>II</sup> (B<sup>III</sup>) cations in OVCs has revealed a one-mode (two-mode) behavior of the low-frequency (high-frequency) vibrational modes.<sup>36,37,42</sup>

In total, we have experimentally resolved 17 modes on DC-CdGa<sub>2</sub>S<sub>4</sub> (taking into account TO-LO splitting). Unfortunately, the LO-TO splitting cannot be distinguished in the experimental B<sup>I</sup> and E<sup>I</sup> modes, and, therefore, a clear comparison with theoretical results cannot be made. Most modes shift to higher frequencies as the pressure increases; however, the low-frequency region modes are almost insensitive to pressure or even show a negative pressure coefficient, like the B<sup>2</sup><sub>TO</sub> and B<sup>2</sup><sub>LO</sub> modes. On the other hand, in the high-frequency region, we observed 9 modes rather overlapped. Therefore, we used *ab initio* calculations in order to help us to assign properly the symmetry of each observed Raman mode (see Fig. 3 and Table I).

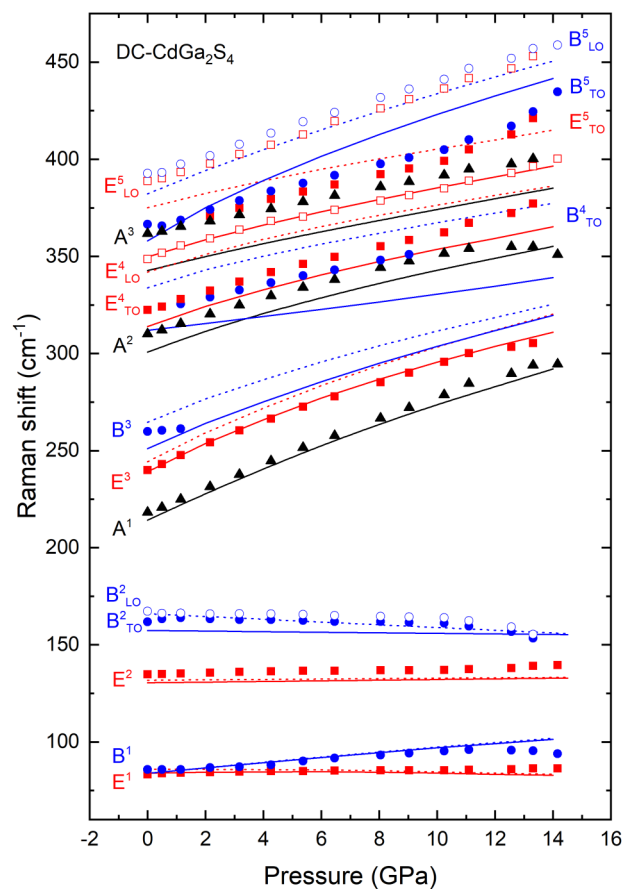


FIG. 3. Pressure dependence of the experimental (symbols) and calculated (lines) vibrational modes in CdGa<sub>2</sub>S<sub>4</sub> up to 14.2 GPa. Experimental values of A, B<sub>TO</sub>/B<sub>LO</sub>, and E<sub>TO</sub>/E<sub>LO</sub> Raman modes are represented by solid triangles (black), solid/open circles (blue), and solid/open squares (red), respectively. Theoretical calculations for the TO (LO) phonons of pure B and E symmetry are represented by solid (dotted) lines with blue and red colors, respectively. In the case of A modes, calculations are shown by solid black lines.

**TABLE I.** Experimental (exp) and theoretical (the) Raman-mode frequencies and their pressure coefficients at room pressure in DC-CdGa<sub>2</sub>S<sub>4</sub> as obtained from fits to the data using equation  $\omega = \omega_0 + aP + bP^2$ , where  $\omega_0$  is expressed in cm<sup>-1</sup>,  $a$  in cm<sup>-1</sup>GPa<sup>-1</sup>, and  $b$  in cm<sup>-1</sup>GPa<sup>-2</sup>. The Grüneisen parameter,  $\gamma_i$ , is also included. Data of other authors are also included for comparison.

Mode (sym.)	$\omega_0$ (the)	$a$ (the)	100· $b$ (the)	$\gamma_i$ (the)	$\omega_0$ (exp)	$a$ (exp)	100· $b$ (exp)	$\gamma_i$ (exp)
B <sup>1</sup> <sub>TO</sub>	83.9 (4) <sup>a</sup> , 121 <sup>b</sup> , 86.0 <sup>c</sup>	1.45 (1) <sup>a</sup> , 0.09 <sup>b</sup> , 1.3 <sup>c</sup>	-1.42 (3) <sup>a</sup> , -1.2 <sup>c</sup>	0.71 (1) <sup>a</sup> , 0.07 <sup>b</sup> , 0.7 <sup>c</sup>	83.5 (1) <sup>a</sup> , 87 <sup>b</sup> , 87 <sup>d</sup>	0.5 (1) <sup>a</sup> , 0.03 <sup>b</sup> , 0.88 <sup>d</sup>	-3 (1) <sup>a</sup> , 0.22 <sup>d</sup>	0.20 (3) <sup>a</sup> , 0.027 <sup>b</sup> , 0.41 <sup>d</sup>
B <sup>1</sup> <sub>LO</sub>	83.9 (3) <sup>a</sup>	1.49 (1) <sup>a</sup>	-1.40 (3)	0.73 (1)				
E <sup>1</sup> <sub>TO</sub>	84.0 (1) <sup>a</sup> , 104 <sup>b</sup> , 86.1 <sup>c</sup>	0.21 (2) <sup>a</sup> , 0.04 <sup>b</sup> , -0.16 <sup>c</sup>	-2.1 (1) <sup>a</sup> , -0.35 <sup>c</sup>	0.10 (1) <sup>a</sup> , 0.03 <sup>b</sup> , -0.09 <sup>c</sup>	85.5 (3) <sup>a</sup> , 84 <sup>b</sup> , 84 <sup>d</sup>	0.40 (2) <sup>a</sup> , 0.04 <sup>b</sup> , 0.63 <sup>d</sup>	8 (2) <sup>a</sup> , -3.62 <sup>d</sup>	0.2 (1) <sup>a</sup> , 0.045 <sup>b</sup> , 0.31 <sup>d</sup>
E <sup>1</sup> <sub>LO</sub>	85.8 (1) <sup>a</sup>	0.06 (2) <sup>a</sup>	-1.7 (1)	0.03 (1)				
E <sup>2</sup> <sub>TO</sub>	130.5 (3) <sup>a</sup> , 125 <sup>b</sup> , 133.1 <sup>c</sup>	0.2 (1) <sup>a</sup> , 0.4 <sup>b</sup> , 0.26 <sup>c</sup>	-0.9 (3) <sup>a</sup> , -1.6 <sup>c</sup>	0.06 (2) <sup>a</sup> , 0.03 <sup>b</sup> , 0.09 <sup>c</sup>	135.1 (2) <sup>a</sup> , 136 <sup>b</sup> , 136 <sup>d</sup>	0.20 (2) <sup>a</sup> , 0.14 <sup>b</sup> , 0.52 <sup>d</sup>	1 (1) <sup>a</sup> , -2.63 <sup>d</sup>	0.05 (3) <sup>a</sup> , 0.09 <sup>b</sup> , 0.16 <sup>d</sup>
E <sup>2</sup> <sub>LO</sub>	131.8 (3) <sup>a</sup>	0.1 (1) <sup>a</sup>	-0.8 (3)	0.03 (2)				
B <sup>2</sup> <sub>TO</sub>	157.5 (2) <sup>a</sup> , 141 <sup>b</sup> , 160.5 <sup>c</sup>	-0.1 (2) <sup>a</sup> , 0.14 <sup>b</sup> , 0.22 <sup>c</sup>	-0.3 (2) <sup>a</sup> , -3.4 <sup>c</sup>	-0.04 (1) <sup>a</sup> , 0.09 <sup>b</sup> , 0.06 <sup>c</sup>	164 (1) <sup>a</sup> , 162 <sup>b</sup> , 162 <sup>d</sup>	-0.30 (2) <sup>a</sup> , 0.03 <sup>b</sup> , -0.03 <sup>d</sup>	1 (2) <sup>a</sup> , -0.38 <sup>d</sup>	-0.08 (3) <sup>a</sup> , 0.02 <sup>b</sup> , -0.008 <sup>d</sup>
B <sup>2</sup> <sub>LO</sub>	165.9 (2) <sup>a</sup>	-0.7 (1) <sup>a</sup>	1.0 (2)	-0.18 (1)	165.8 (4) <sup>a</sup> , 168 <sup>b</sup> , 168 <sup>d</sup>	0.2 (2) <sup>a</sup> , 0.17 <sup>b</sup> , -0.02 <sup>d</sup>	-4 (1) <sup>a</sup> , -4.65 <sup>d</sup>	0.05 (2) <sup>a</sup> , 0.09 <sup>b</sup> , -0.005 <sup>d</sup>
A <sup>1</sup>	214.9 (4) <sup>a</sup> , 194 <sup>b</sup> , 213.6 <sup>c</sup>	6.7 (1) <sup>a</sup> , 1.54 <sup>b</sup> , 6.2 <sup>c</sup>	-7.9 (4) <sup>a</sup> , -7.0 <sup>c</sup>	1.26 (3) <sup>a</sup> , 0.70 <sup>b</sup> , 1.34 <sup>c</sup>	217 (1) <sup>a</sup> , 219 <sup>b</sup> , 219 <sup>d</sup>	7.0 (2) <sup>a</sup> , 5.82 <sup>b</sup> , 6.36 <sup>d</sup>	-10 (1) <sup>a</sup> , -1.62 <sup>d</sup>	1.3 (1) <sup>a</sup> , 2.34 <sup>b</sup> , 1.18 <sup>d</sup>
E <sup>3</sup> <sub>TO</sub>	241 (1) <sup>a</sup> , 241 <sup>b</sup> , 247.5 <sup>c</sup>	6.5 (1) <sup>a</sup> , 3.26 <sup>b</sup> , 6.4 <sup>c</sup>	-10 (1) <sup>a</sup> , -10.5 <sup>c</sup>	1.11 (4) <sup>a</sup> , 1.19 <sup>b</sup> , 1.2 <sup>c</sup>	239.9 (4) <sup>a</sup> , 241 <sup>b</sup> , 242 <sup>d</sup>	6.9 (1) <sup>a</sup> , 5.42 <sup>b</sup> , 6.54 <sup>d</sup>	-14 (1) <sup>a</sup> , -8.5 <sup>d</sup>	1.17 (4) <sup>a</sup> , 1.98 <sup>b</sup> , 1.10 <sup>d</sup>
E <sup>3</sup> <sub>LO</sub>	246 (1) <sup>a</sup>	6.8 (1) <sup>a</sup>	-10 (1)	1.12 (3)	245 <sup>b</sup>	5.26 <sup>d</sup>		
B <sup>3</sup> <sub>TO</sub>	252 (1) <sup>a</sup> , 259 <sup>b</sup> , 257.8 <sup>c</sup>	5.9 (1) <sup>a</sup> , 2.6 <sup>b</sup> , 5.7 <sup>c</sup>	-7 (1) <sup>a</sup> , -8.4 <sup>c</sup>	0.95 (3) <sup>a</sup> , 0.89 <sup>b</sup> , 1.0 <sup>c</sup>	259.9 (1) <sup>a</sup> , 261 <sup>d</sup>	1.2 (1) <sup>a</sup> , 2.07 <sup>d</sup>		0.19 (2) <sup>a</sup> , 0.32 <sup>d</sup>
B <sup>3</sup> <sub>LO</sub>	266 (1) <sup>a</sup>	5.2 (1) <sup>a</sup>	-6 (1)	0.79 (3)				
A <sup>2</sup>	302 (1) <sup>a</sup> , 296 <sup>b</sup> , 307.9 <sup>c</sup>	4.7 (1) <sup>a</sup> , 3.6 <sup>b</sup> , 4.6 <sup>c</sup>	-6 (1) <sup>a</sup> , -7.4 <sup>c</sup>	0.63 (2) <sup>a</sup> , 1.06 <sup>b</sup> , 0.69 <sup>c</sup>	309.9 (1) <sup>a</sup> , 311 <sup>b</sup> , 311 <sup>d</sup>	5.0 (2) <sup>a</sup> , 4.45 <sup>b</sup> , 4.72 <sup>d</sup>	-9.3 (4) <sup>a</sup> , -5.73 <sup>d</sup>	0.66 (1) <sup>a</sup> , 1.26 <sup>b</sup> , 0.62 <sup>d</sup>
B <sup>4</sup> <sub>TO</sub>	312 (1) <sup>a</sup> , 352 <sup>b</sup> , 313.2 <sup>c</sup>	1.7 (1) <sup>a</sup> , 4.3 <sup>b</sup> , 1.5 <sup>c</sup>	1.9 (1) <sup>a</sup> , -0.73 <sup>c</sup>	0.22 (3) <sup>a</sup> , 1.07 <sup>b</sup> , 0.22 <sup>c</sup>	324 (1) <sup>a</sup> , 325 <sup>b</sup> , 323 <sup>d</sup>	2.8 (1) <sup>a</sup> , 2.33 <sup>b</sup> , 2.29 <sup>d</sup>		0.36 (2) <sup>a</sup> , 0.63 <sup>b</sup> , 0.29 <sup>d</sup>
E <sup>4</sup> <sub>TO</sub>	315 (1) <sup>a</sup> , 356 <sup>b</sup> , 321 <sup>c</sup>	4.3 (1) <sup>a</sup> , 4.3 <sup>b</sup> , 4.2 <sup>c</sup>	-5 (1) <sup>a</sup> , -6 <sup>c</sup>	0.56 (2) <sup>a</sup> , 1.06 <sup>b</sup> , 0.60 <sup>c</sup>	322 (3) <sup>a</sup> , 323 <sup>b</sup> , 322 <sup>d</sup>	4.9 (2) <sup>a</sup> , 4.29 <sup>b</sup> , 4.89 <sup>d</sup>	-9 (2) <sup>a</sup> , -8.07 <sup>d</sup>	0.62 (3) <sup>a</sup> , 1.17 <sup>b</sup> , 0.62 <sup>d</sup>
B <sup>4</sup> <sub>LO</sub>	335 (1) <sup>a</sup>	3.6 (1) <sup>a</sup>	-4 (1) <sup>a</sup>	0.44 (2) <sup>a</sup>				
E <sup>4</sup> <sub>LO</sub>	343.0 (1) <sup>a</sup>	3.9 (1) <sup>a</sup>	-5 (1) <sup>a</sup>	0.46 (2) <sup>a</sup>	350 (1) <sup>a</sup> , 350 <sup>b</sup> , 351 <sup>d</sup>	4.0 (3) <sup>a</sup> , 3.94 <sup>b</sup> , 4.4 <sup>d</sup>	-5 (2) <sup>a</sup> , -9.8 <sup>d</sup>	0.47 (2) <sup>a</sup> , 0.99 <sup>b</sup> , 0.51 <sup>d</sup>
A <sup>3</sup>	343.3 (2) <sup>a</sup> , 343 <sup>b</sup> , 346 <sup>c</sup>	3.3 (1) <sup>a</sup> , 3.9 <sup>b</sup> , 3.0 <sup>c</sup>	-2.3 (2) <sup>a</sup> , -2.1 <sup>c</sup>	0.40 (5) <sup>a</sup> , 1.00 <sup>b</sup> , 0.40 <sup>c</sup>	361 (1) <sup>a</sup> , 361 <sup>b</sup> , 362 <sup>d</sup>	3.3 (1) <sup>a</sup> , 3.32 <sup>b</sup> , 3.66 <sup>d</sup>	-4 (1) <sup>a</sup> , -5.96 <sup>d</sup>	0.38 (2) <sup>a</sup> , 0.81 <sup>b</sup> , 0.41 <sup>d</sup>
E <sup>5</sup> <sub>TO</sub>	351 (1) <sup>a</sup> , 402 <sup>b</sup> , 357.5 <sup>c</sup>	3.8 (1) <sup>a</sup> , 4.7 <sup>b</sup> , 3.7 <sup>c</sup>	-3.6 (4) <sup>a</sup> , -4 <sup>c</sup>	0.43 (1) <sup>a</sup> , 1.03 <sup>b</sup> , 0.48 <sup>c</sup>	361 (2) <sup>a</sup> , 367 <sup>b</sup> , 366 <sup>d</sup>	4.6 (2) <sup>a</sup> , 6.38 <sup>b</sup> , 3.49 <sup>d</sup>	-9 (2) <sup>a</sup> , -1.48 <sup>d</sup>	0.52 (2) <sup>a</sup> , 1.53 <sup>b</sup> , 0.39 <sup>d</sup>
B <sup>5</sup> <sub>TO</sub>	360 (1) <sup>a</sup> , 412 <sup>b</sup> , 368.9 <sup>c</sup>	7.3 (1) <sup>a</sup> , 4.7 <sup>b</sup> , 6.8 <sup>c</sup>	-10.5 (4) <sup>a</sup> , -10.1 <sup>c</sup>	0.83 (1) <sup>a</sup> , 1.00 <sup>b</sup> , 0.85 <sup>c</sup>	363 (3) <sup>a</sup> , 364 <sup>b</sup> , 367 <sup>d</sup>	5.3 (2) <sup>a</sup> , 6.33 <sup>b</sup> , 7.02 <sup>d</sup>	-13 (2) <sup>a</sup> , -18.5 <sup>d</sup>	0.60 (2) <sup>a</sup> , 1.53 <sup>b</sup> , 0.78 <sup>d</sup>
E <sup>5</sup> <sub>LO</sub>	376 (1) <sup>a</sup>	3.2 (2) <sup>a</sup>	-3 (1) <sup>a</sup>	0.35 (1) <sup>a</sup>	388 (1) <sup>a</sup> , 390 <sup>b</sup> , 389 <sup>d</sup>	4.5 (2) <sup>a</sup> , 4.79 <sup>b</sup> , 5.71 <sup>d</sup>	2 (1) <sup>a</sup> , -8.16 <sup>d</sup>	0.48 (3) <sup>a</sup> , 1.08 <sup>b</sup> , 0.60 <sup>d</sup>
B <sup>5</sup> <sub>LO</sub>	383 (2) <sup>a</sup>	5.7 (1) <sup>a</sup>	-6.1 (2) <sup>a</sup>	0.61 (1) <sup>a</sup>	392 (1) <sup>a</sup> , 393 <sup>b</sup> , 394 <sup>d</sup>	5.2 (2) <sup>a</sup> , 5.62 <sup>b</sup> , 5.71 <sup>d</sup>	-2 (1) <sup>a</sup> , -6.93 <sup>d</sup>	0.54 (2) <sup>a</sup> , 1.26 <sup>b</sup> , 0.59 <sup>d</sup>

<sup>a</sup>This work.

<sup>b</sup>Ref. 27 ( $a$  calculated using  $B_0 = 88$  GPa).

<sup>c</sup>Ref. 28 ( $\gamma_i$  calculated using  $B_0 = 46$  GPa).

<sup>d</sup>Ref. 26 ( $\gamma_i$  calculated using  $B_0 = 40.6$  GPa).

Notably, neither our unpolarised RS spectra at room temperature nor those of Ursaki *et al.*<sup>26</sup> and Mitani *et al.*<sup>27</sup> show the B<sup>1</sup><sub>LO</sub>, E<sup>1</sup><sub>LO</sub>, E<sup>2</sup><sub>LO</sub>, E<sup>3</sup><sub>LO</sub>, B<sup>3</sup><sub>LO</sub>, and B<sup>4</sup><sub>LO</sub> modes. For the B<sup>1</sup>, E<sup>1</sup>, and E<sup>2</sup> modes, our *ab initio* calculations indicate that the LO-TO splitting

is too small to be distinguished with the resolution of our RS measurements. However, this explanation is not valid for the E<sup>3</sup><sub>LO</sub>, B<sup>3</sup><sub>LO</sub>, and B<sup>4</sup><sub>LO</sub> modes. Since these modes were observed in DC-CdGa<sub>2</sub>S<sub>4</sub> by Nebola *et al.*<sup>43</sup> and Syrbu *et al.*<sup>44</sup> for  $z(yx)y$

orientation in polarized RS measurements, we think that polarized RS measurements are required to observe such modes.

Other relevant features of our RS spectra are the low intensities and large linewidths of some Raman modes, which lead to the appearance or disappearance of these modes at different pressures. For example, the weak  $B^3$  mode disappears above 1 GPa because it overlaps with the strong  $E^3$  mode, as also noted in Refs. 26 and 27. The situation is even more complex in the high-frequency region, where Mitani *et al.*<sup>27</sup> observed the emergence of the  $B^4$  (near 330  $\text{cm}^{-1}$ ) and  $E^5$  (near 370  $\text{cm}^{-1}$ ) modes at 1.43 and 1.25 GPa, respectively. Thanks to our calculations, we have resolved that these two emerging modes correspond to the  $B^4_{TO}$  and  $E^5_{TO}$  modes. The massive overlapping in the high-frequency region makes difficult to distinguish them at room pressure.

To finish the discussion of Fig. 2, we must consider that Raman peaks were measured up to 14.2 GPa. Above 15 GPa, no signal in Raman spectra is observed, thus evidencing the PT to a Raman-inactive phase. This PT pressure is in accordance with the results of Ursaki *et al.* and Mitani *et al.*<sup>26,27</sup> We have assigned the HP phase to a DR structure [Fig. 1(c)] according to HP-XRD measurements that observed a PT to the DR phase above 17 GPa.<sup>22</sup> It must be said that several photographs of the sample were taken in order to follow the changes on its colour under compression. In this respect, we observed some dark zones on the sample at 14.2 GPa and found that the sample was totally opaque when we reached the maximum pressure of this study (25 GPa). These results provide evidence of the stability range of the ordered (transparent) and fully disordered (opaque) phases, as have been previously observed in other OVCs.<sup>15,18,20</sup>

Figure 3 shows the pressure dependence of the experimental and theoretical Raman mode frequencies of DC-CdGa<sub>2</sub>S<sub>4</sub> up to 14 GPa. At a glance, the comparison of *ab initio* calculations and measurements shows a rather good agreement of the frequencies and pressure coefficients, but a slight underestimation of the theoretical Raman frequencies. In general, the  $E$  modes are better described than the  $A$  and  $B$  modes and the agreement between experimental and theoretical frequencies in absolute value is much better in the low- and medium-frequency regions. Table I summarizes the experimental and theoretical zero-pressure Raman-active mode frequencies ( $\omega_0$ ) and their pressure coefficients ( $a$  and  $b$ , linear and quadratic terms, respectively). Experimental and theoretical results from Refs. 26–28 are also shown for comparison. Analysis of data in Table I indicate that our experimental frequencies and linear pressure coefficients agree quite well with those of Refs. 26 and 27, being the agreement better for the Raman modes of the high- and medium-frequency regions, except for the  $E^5_{TO}$  and  $B^5_{TO}$  mode. On the other hand, our theoretical frequencies and pressure coefficients agree rather well with our experimental results. Additionally, our theoretical TO modes agree with *ab initio* calculations of Ref. 28, but show considerable deviation with the lattice dynamics calculations of Ref. 27 which are based on the Harrison-Keating model. In quantitative terms, we have found an average relative error between our calculations and our experiments of less than 5% in the Raman-mode frequencies and less than 10% in  $a$  parameters in the medium and high-frequency regions. The largest relative errors are found in the low-frequency region, except for the case of the  $B^3_{TO}$  and  $B^4_{TO}$  modes in the medium- and high-frequency

regions, respectively. The reasons for the discrepancies could be the small pressure region in which the  $B^3_{TO}$  mode is experimentally observed and problems with *ab initio* calculations for the  $B^4_{TO}$  mode (see Fig. 3), whose theoretical  $a$  value is anomalously low in comparison with the rest of the high-frequency modes. Finally, our experimental and theoretical Grüneisen parameters will be discussed in detail in Sec. V in relation to the calculation of the heat capacity and the thermal expansion coefficient.

It is worth noting the anomalous changes on the trends of some Raman modes above 10–11 GPa; i.e., prior to the pressure-induced PT to the DR phase. In particular, we have noticed a decrease of the pressure coefficient of the  $A^2$  mode and an increase of the pressure coefficient of the TO modes  $E^4_{TO}$ ,  $E^5_{TO}$ , and  $B^5_{TO}$  that makes them to approach to their respective LO counterparts at a much larger rate than at lower pressures. It is well known that the LO-TO splitting in most ionic (or polar) semiconductors, such as ZB-type InAs, InP, GaSb, GaAs, and GaP,<sup>45–48</sup> decreases under pressure due to the decrease of the ionic character of the cation-anion bonds, which leads to a decrease of the Born effective charges.<sup>45–48</sup> Therefore, the decrease of the LO-TO splitting observed in our RS measurements indicate a decrease of the ionicity in DC-CdGa<sub>2</sub>S<sub>4</sub> at HP that is more significant above 10–11 GPa. This decrease of the ionicity in DC-CdGa<sub>2</sub>S<sub>4</sub> is in good agreement with recent theoretical studies on the elastic properties of DC-HgGa<sub>2</sub>Se<sub>4</sub> and DC-HgGa<sub>2</sub>S<sub>4</sub> at HP that show that their Poisson's ratio increases at HP (especially quick close to the PT), thus indicating a decrease of the ionic character of these DC-type compounds under compression.<sup>2,49,50</sup>

It must be mentioned that the steep increase of the frequency in some high-frequency modes at pressures close to the PT was also observed by Mitani *et al.* above 9 GPa,<sup>27</sup> but not by Ursaki *et al.*<sup>26</sup> A possible explanation regarding this discordance could be the different crystal growth methods used by Ursaki *et al.* (the chemical transport method)<sup>26</sup> and by Mitani *et al.* (the Bridgman method).<sup>27</sup> However, we have observed the same behaviour of the high-frequency modes as Mitani *et al.* in samples synthesized with the chemical transport method. Consequently, we may speculate that this feature could be associated with non-hydrostatic stresses, which could appear when using methanol-ethanol around 10 GPa, or with a different initial degree of tetragonal distortion of the original samples, regardless of the crystal growth method.<sup>27,51</sup>

Let us now concentrate on the discussion of the two order-disorder stages which could occur prior to the DC-to-DR PT, as proposed in previous HP studies of OVCs. These two possible stages are first, a disorder between both cations and, second, a disorder between both cations and vacancies. In this context, several studies on OVCs at room pressure have pointed out that the existence of disorder in the cation sublattice could be traced by the broadening observed on some Raman peaks.<sup>52</sup> For instance, this broadening was observed in Zn<sub>1-x</sub>Mn<sub>x</sub>Ga<sub>2</sub>Se<sub>4</sub> crystals for  $x < 1$  and was attributed to the partially disordered cation arrangement.<sup>53</sup> On the other hand, the RS spectra of ZnGa<sub>2</sub>Se<sub>4</sub> and CdGa<sub>2</sub>Se<sub>4</sub> compounds at 570 K in comparison with those taken at 300 K also exhibited a general broadening of some Raman peaks.<sup>54</sup> Notably, Refs. 53 and 54 share a common feature: a considerable intensity decrease of the  $A^1$  mode.

In order to evaluate the existence of the order-disorder stages on CdGa<sub>2</sub>S<sub>4</sub> at HP, Ursaki *et al.*<sup>26</sup> and Mitani *et al.*<sup>27</sup> analyzed the intensity and full width at half maximum (FWHM) of different

Raman modes. Ursaki *et al.* observed a remarkable increase of the FWHM of the Raman modes and a decrease of the intensity of the  $A^2$  mode above 8 GPa, whereas the intensity of most other Raman modes started to decrease at around 10 GPa (the most notorious case is that of the  $A^1$  mode). These pressures were assigned as the onsets of the first and second stages of disorder, respectively. On the other hand, Mitani *et al.* suggested that the first stage of disorder corresponds to the change in the FWHM of the  $A^1$  mode above 6 GPa and the second stage of disorder corresponds to the increase of the FWHM of the modes above 8 GPa. In summary, there exists several changes in the RS spectra that could indicate the existence of two order-disorder stages, but there is no agreement in the pressure for the onset of such stages. In this context, we have to mention that the assumption that the two stages of order-disorder should occur at HP are based on high temperature studies of OVCs;<sup>55</sup> hence, extrapolating them to HP conditions at room temperature might lead to misinterpretations.

In order to clarify the presence of the order-disorder stages during compression in DC-CdGa<sub>2</sub>S<sub>4</sub>, we have also analyzed the HP dependence of the FWHM (Fig. 4) and intensity (Fig. 5) of well-observed Raman modes. Regarding the FWHMs, an increase

(decrease) of the FWHM of the  $E^1$  and  $E^2$  ( $A^1$ ) modes occurs above 9 GPa and a general increase of the FWHMs is observed above 12 GPa. Regarding the intensities, we have plotted, on one hand, the absolute intensity of the  $A^1$  mode and, on the other hand, the intensity of the other Raman modes normalized to that of the  $A^1$  mode for each pressure value. The relative intensity of  $E^1$ ,  $E^2$ , and  $A^2$  modes increases up to 9–10 GPa and drops slightly above that pressure. On the other hand, the intensity of the  $E^4_{TO}$  mode drops gradually and the  $B^4_{TO}$  mode disappears above 9 GPa. Finally, the  $A^1$  mode intensity does not significantly change up to this pressure and only decreases abruptly above 12 GPa.

These changes can be understood if we consider that the first stage of disorder, involving only cation disorder, leads to a DS structure, which is more symmetric than the DC phase and consequently has one  $A$  mode less than the DC phase.<sup>56</sup> The DS unit cell can be displayed as the DC one in which cations in Cd-Ga planes are randomly disordered between Cd and Ga sites; i.e., they have a fractional occupation factor (DS model 6 in Ref. 56). In particular, the decrease of intensity and disappearance of the  $A^2$  mode in DC-CdGa<sub>2</sub>Se<sub>4</sub> above 8 GPa and in DC-CdAl<sub>2</sub>S<sub>4</sub> above 6 GPa,

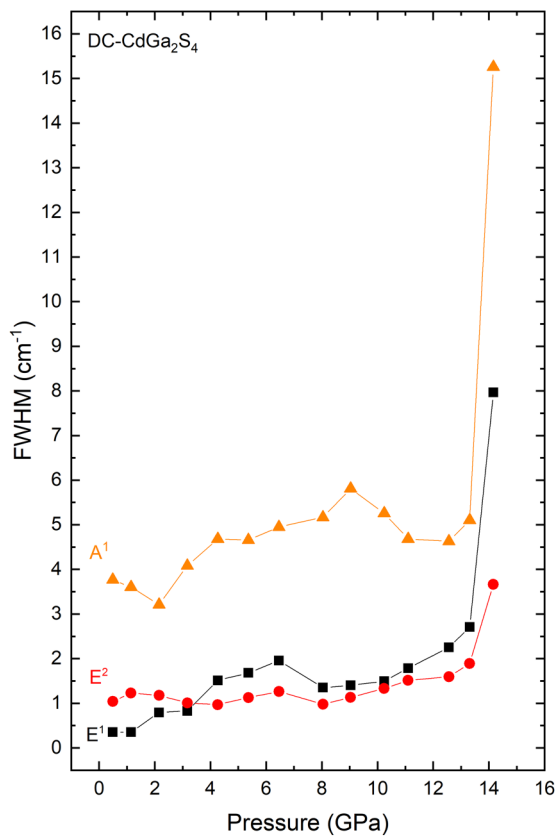


FIG. 4. FWHM of the  $E^1$ ,  $E^2$ , and  $A^1$  modes of DC-CdGa<sub>2</sub>S<sub>4</sub> during the first upstroke. Solid straight lines are a guide to the eyes.

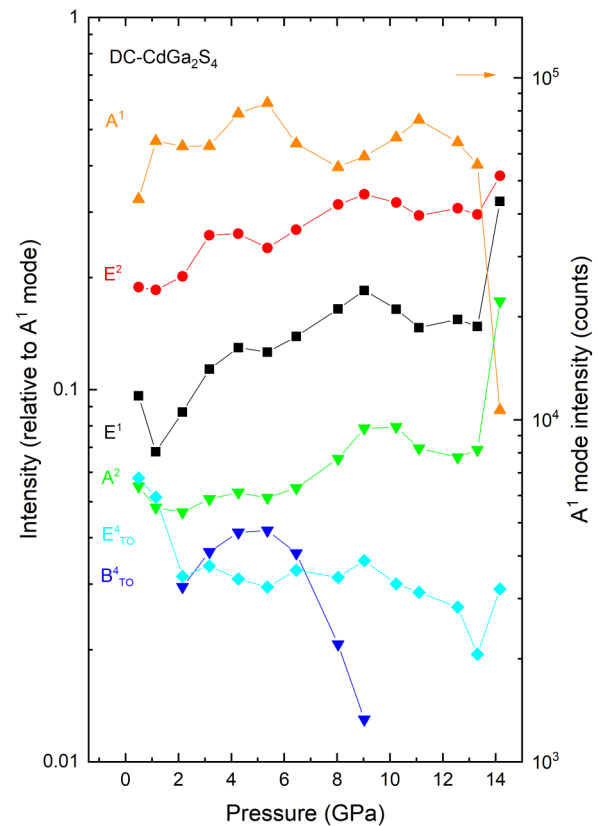


FIG. 5. Pressure dependence of the intensity of the  $A^1$  mode (right vertical axis) and  $E^1$ ,  $E^2$ ,  $A^2$ ,  $E^4_{TO}$ , and  $B^4_{TO}$  modes (left vertical axis). In the left vertical axis, intensities are normalized to that of the  $A^1$  mode. Solid straight lines are a guide to the eyes.



respectively, was attributed to DC-to-DS PT.<sup>15,16</sup> Since we have also observed changes in the  $A^2$  mode in DC- $\text{CdGa}_2\text{S}_4$  above 9 GPa that are correlated with changes in the intensities, FWHMs and frequencies of different Raman modes at similar pressures, we conclude that the onset of the first order-disorder stage occurs above 9 GPa in DC- $\text{CdGa}_2\text{S}_4$ .

On the other hand, we have found no evidences for a second order-disorder stage. The second order-disorder stage involves disorder in both cation and vacancy sites. This disorder in a tetrahedrally-coordinated structure would lead to a DZ phase in  $\text{CdGa}_2\text{S}_4$ , where both Cd and Ga cations and vacancies are all mixed in cation sites; i.e., with a complete disorder in cation sites.<sup>56</sup> Since cubic ZB-type compounds are more symmetric than tetragonal DC and DS phases, they have only 3 Raman-active modes: the LO mode plus the doubly degenerated TO mode. This result is not consistent with our RS measurements during the first upstroke where much more than 2 Raman peaks are clearly observed prior to the almost complete disappearance of the Raman signal above 15 GPa. Consequently, we can conclude that there is no evidence for a second order-disorder stage, unlike proposed by Ursaki *et al.*<sup>26</sup> and Mitani *et al.*<sup>27</sup>

## B. Second upstroke

In order to study the reversibility of the DC-to-DR PT and the stability of the DR phase upon decompression, we decompressed our diamond anvil cell from 25 GPa down to 1.8 GPa at a slow rate because the rate of decompression, together with temperature, plays an important role in the quenching of HP phases in OVCs.<sup>17,26,57,58</sup> Figure 6 displays the RS spectrum at 1.8 GPa and its evolution on increasing pressure during a second upstroke up to 21.5 GPa. The recovered sample at 1.8 GPa shows broad Raman bands and is not transparent as the initial DC phase. Therefore, it is clear that we did not recover the DC phase on decompression, unlike it was suggested in Refs. 26 and 27. In this context, a DZ phase was observed upon a slow decompression in other OVCs, like DC- $\text{CdGa}_2\text{Se}_4$  and DC- $\text{HgGa}_2\text{S}_4$ .<sup>20,21</sup> They exhibited several broad bands similar to those of our RS spectrum at 1.8 GPa. Consequently, based on earlier HP studies, we have assigned the RS spectrum at 1.8 GPa to the DZ phase, where anions are at 4c sites and cations and vacancies are totally disordered at 4a sites [Fig. 1(d)]. Further support to our hypothesis is provided in Ref. 25, where a RS spectrum of DZ- $\text{CdGa}_2\text{S}_4$ , similar to that of our recovered sample at 1.8 GPa, was observed under Berkovich indentation mixed with initial DC- $\text{CdGa}_2\text{S}_4$  (see Fig. 10 in Ref. 25).

We must recall that the RS spectrum of DZ- $\text{CdGa}_2\text{S}_4$  consists of several broad bands that cannot be considered the 3 Raman-active modes of the ZB structure. Indeed, what can be observed is a disorder-activated Raman scattering (DARS) that occurs in disordered samples and reveals the one-phonon density of states of the DZ structure.<sup>59,60</sup> In Fig. 6, we have marked by arrows (from 1 to 7) the different Raman bands at 1.8 GPa whose pressure dependence has been followed. As can be observed, the DZ phase persists up to 9.7 GPa and the Raman-inactive DR phase appears above that pressure, in good agreement with the pressure-induced transition from the ZB to the rock salt phase observed in compounds, like ZnSe, ZnS, InP, or InAs.<sup>61</sup>

To the best of our knowledge, Ursaki *et al.* were the first to perform a second upstroke on  $\text{CdGa}_2\text{S}_4$ .<sup>26</sup> They assigned an amorphous DC phase on decompression for two reasons: (i) a peak around  $200\text{ cm}^{-1}$  that resembles the  $A^1$  mode of the DC phase; (ii) several narrow bands appearing at low frequencies on increasing pressure to 4.7 GPa were attributed to the recrystallization of the DC phase. On the other hand, their recovered sample underwent a PT to the DR phase above 7.7 GPa in the second upstroke. Contrarily, we did not observe other new Raman peaks in our recovered sample on increasing pressure and the Raman signal persisted up to upper pressures (9.7 GPa) in the second upstroke. The discrepancy between our RS measurements and those of Ursaki *et al.* can be understood if we consider that the recovered sample in the two measurements was obtained upon decreasing pressure from two different pressures. In the experiment of Ursaki *et al.*, the sample was decompressed from 15 GPa, so the narrow modes observed in the recovered sample could be attributed to the DS phase if we assume that the DS-to-DR PT was not fully completed at 15 GPa. On the other hand, in our experiment, the sample was decompressed from 25 GPa; therefore, the DS-to-DR PT was fully

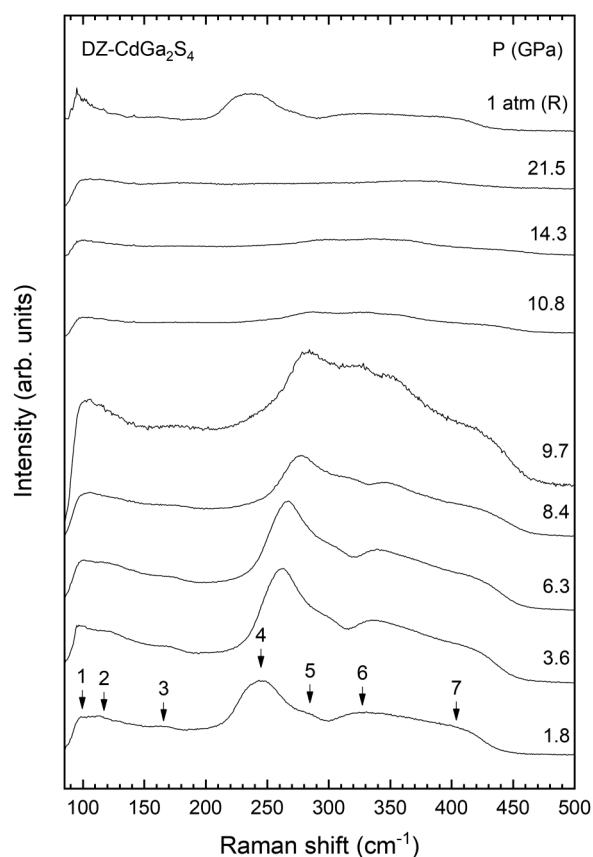


FIG. 6. Room temperature Raman scattering spectra of DZ- $\text{CdGa}_2\text{S}_4$  up to 21.5 GPa. The Raman spectrum of the recovered sample at 1 atm is shown at the top.

accomplished and the recovered sample corresponds to the completely disorder DZ phase.

On downstroke from 21.5 GPa, we slowly decreased the pressure down to 1 atm (see top RS spectrum of Fig. 6) in order to check the reversibility of the DZ-to-DR PT. As observed, the RS spectrum at 1 atm after the second upstroke is similar to the RS spectrum of DZ-CdGa<sub>2</sub>S<sub>4</sub> at 1.8 GPa recovered from the first upstroke. Therefore, we can conclude that the DZ-to-DR PT is a reversible one; i.e., our results show the inability of the fully disordered phases of CdGa<sub>2</sub>S<sub>4</sub> to transform to an ordered phase under compression or decompression. In fact, fully disorder-order transitions have been observed in many OVCs under cooling during crystal growth, where the control of the temperature leads to avoid cracking defects.<sup>62</sup> In summary, our measurements have clearly shown that there is an irreversible DC-to-DR PT on increasing pressure above 15 GPa which proceeds via an intermediate DS

phase above 9 GPa. On decreasing pressure from the DR phase, a DZ phase that undergoes a reversible DZ-to-DR PT is obtained.

Figure 7 shows the pressure dependence of the seven vibrational modes of DZ-CdGa<sub>2</sub>S<sub>4</sub>. Table II shows the experimental Raman mode frequencies and their pressure coefficients at room pressure for the DZ phase. The Raman modes of the DZ phase shift to high pressures with a linear trend, but with smaller pressure coefficients than those of the DC phase. This result shows the effect of the disorder in the pressure dependence of the Raman wavenumbers; i.e., the larger the disorder, the smaller the pressure coefficients.<sup>20</sup> In fact, the analysis of the effect of pressure on the RS spectrum of the recovered sample from Ursaki *et al.* shows that the pressure coefficient of the most intense mode, which resembles to the A<sup>1</sup> mode of the DC phase, is around 6.5 cm<sup>-1</sup>GPa<sup>-1</sup>. This value is between the pressure coefficient of the A<sup>1</sup> mode in the DC phase (7.0 cm<sup>-1</sup>GPa<sup>-1</sup>) and that of the band 4 of the DZ phase (3.7 cm<sup>-1</sup>GPa<sup>-1</sup>). Therefore, our analysis suggests the presence of the DS phase in the recovered sample of Ursaki *et al.* in the first upstroke. Moreover, one can notice that the narrow bands in the RS spectrum of the recovered sample of Ursaki *et al.* are on top of a broad RS spectrum (see Fig. 10 in Ref. 26) that is similar to that of our DZ phase at 1.8 GPa (see Fig. 6) above 220 cm<sup>-1</sup>. Therefore, we can conclude that the recovered sample of Ursaki *et al.* in the first upstroke was a mixture of DS and DZ phases and not an amorphous DC phase.

As already commented, the RS spectrum of DZ-CdGa<sub>2</sub>S<sub>4</sub> resembles the one-phonon density of states of ZB-type compounds, and in particular of ZnS in the case of CdGa<sub>2</sub>S<sub>4</sub>,<sup>63–65</sup> due to the similarity of the mass of Zn (65.39 uma) and the cation average mass (2 Ga + 1 Cd + 1 vacancy) in DZ-CdGa<sub>2</sub>S<sub>4</sub> (62.96 uma). However, the modes of DZ-CdGa<sub>2</sub>S<sub>4</sub> spread out in the same range of frequencies (up to 430 cm<sup>-1</sup>) of the DC phase, unlike in ZnS (up to 370 cm<sup>-1</sup>). The above features allow us to make a correlation in terms of frequency between the modes of the DZ and the DC phase with the ZB-type ZnS by folding the phonon dispersion curves of ZnS into the BZ center.<sup>1,66</sup> Moreover, the phonon density of states for ZnS allows us to assign the TA, LA, TO, and LO mode character of the Raman bands of the DZ phase.<sup>64,67</sup>

In DZ-CdGa<sub>2</sub>S<sub>4</sub>, bands 1 and 2 correspond to the E<sup>1</sup>, B<sup>1</sup>, and E<sup>2</sup> modes in the DC phase that have a TA mode character. The frequency of band 3 matches with the B<sup>2</sup><sub>TO</sub> and B<sup>2</sup><sub>LO</sub> modes of DC phase and has LA mode character. Above 250 cm<sup>-1</sup>, bands 5 and 6

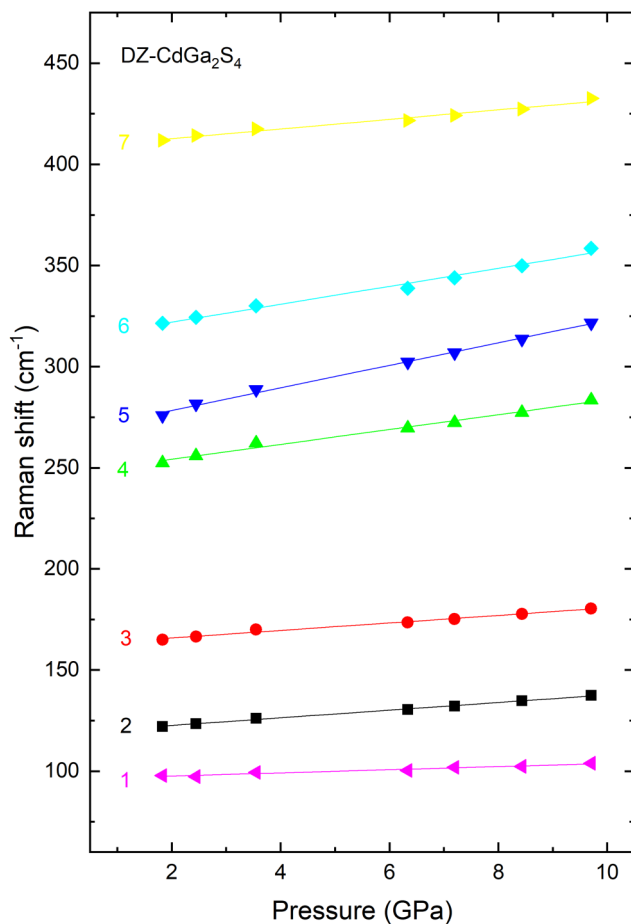


FIG. 7. Pressure dependence of the experimental (symbols) frequencies of Raman-active modes in DZ-CdGa<sub>2</sub>S<sub>4</sub> during the 2nd upstroke. Solid lines correspond to linear fits to experimental data.

TABLE II. Experimental Raman-mode frequencies and their pressure coefficients at room pressure in DZ-CdGa<sub>2</sub>S<sub>4</sub> as obtained from fits to the data using equation  $\omega = \omega_0 + aP$ , where  $\omega_0$  is expressed in cm<sup>-1</sup> and  $a$  in cm<sup>-1</sup>GPa<sup>-1</sup>.

Peak	$\omega_0$	$a$
1	96.0 (5)	0.8 (1)
2	118.8 (3)	1.9 (1)
3	162.1 (6)	1.9 (1)
4	247 (1)	3.7 (2)
5	267 (1)	5.6 (2)
6	313 (2)	4.4 (2)
7	408 (1)	2.4 (2)

are close in frequency to the  $E^3$ ,  $B^3$ ,  $A^2$ ,  $B^4_{TO}$ , and  $E^4_{TO}$  modes in the DC phase. Since the phonon density of states of the TO modes at the BZ center of the ZnS covers these latter bands in the DZ phase, we assign to bands 5 and 6 a TO mode character. The broad band 7 is in the range defined by the  $E^4_{LO}$  and  $B^5_{LO}$  modes in the DC phase with LO mode character. Note that band 7 is the highest in frequency and falls into the narrow phonon density of states of LO modes of ZnS, which are centered at  $370\text{ cm}^{-1}$ .<sup>64</sup> We think that the large broadening of band 7, which extends up to much larger frequencies than in ZnS, can be explained by the LO two-mode phonon behavior of the modes in the high-frequency region, already observed in mixed DC compounds.<sup>37,42,68</sup> In this context, the mixture of LO modes corresponding to stretching vibrations of S anions against Cd cations, Ga cations, and vacancies would explain that the low-frequency edge ( $350\text{ cm}^{-1}$ ) of this broad LO band in the DZ phase corresponds to the Cd-S stretching mode near the BZ zone center, while the high-frequency edge corresponds to the vacancy-S stretching mode. Finally, band 4 of the DZ phase, which has the highest intensity, is quite similar to the  $A^1$  mode of the DC phase, which is related to the breathing vibration of S atoms against the vacancies. Band 4 cannot be correlated neither with LA nor TO character because it is located in the gap of the phonon density of states of ZnS between acoustic and optic modes, what confirms the non-polar character of this band. This is a remarkable feature since the presence of this band of the DZ phase related to the presence of vacancies cannot be deduced from those of the ZB phase in common binary  $AX$  compounds.

## V. GRÜNEISEN PARAMETER AND THERMAL PROPERTIES

The use of the Grüneisen parameter to calculate thermal and elastic properties of materials allows circumventing some experimental limitations on direct measurements of these properties. For instance, the determination of the pressure dependence of the thermal conductivity of materials is a common technological issue, requiring the use of thermal contacts which are not always feasible.<sup>68,69</sup> The Grüneisen parameter provides the asymmetry of the vibration of the atoms from their equilibrium position, giving information on the anharmonicity of the crystal.<sup>70–72</sup> It must be considered for properties that depend directly on the anharmonicity of the crystal potential energy, i.e., thermal expansion, deviations from Debye's specific heat at high temperatures, and thermal conductivity in insulators.<sup>73</sup> In addition, a correlation between the negative Grüneisen parameter of the TA phonon at the X point of the BZ and the PT pressure for various  $A$ ,  $AX$ , and  $ABX_2$ -type semiconductors has been studied.<sup>74</sup> Furthermore, under quasi-harmonic conditions, one can determine the molar heat capacity ( $C_v$ ) and the thermal expansion coefficient ( $\alpha$ ) by using the pressure or volume derivatives of the phonon frequencies at the BZ center, thanks to the Grüneisen parameter.<sup>69</sup>

In this work, we will work with two formulations of the Grüneisen parameter ( $\gamma$ ): the microscopic Grüneisen parameter,<sup>75</sup> defined by Grüneisen for a quasi-harmonic mode of frequency  $\omega_i$  as  $\gamma_i = (B_0/\omega_i)(d\omega_i/dP)$  where  $B_0$  is the isothermal bulk modulus, and the macroscopic Grüneisen parameter (or average Grüneisen parameter),<sup>73</sup> which is expressed in terms of  $\alpha$ ,  $C_v$ , and molar

volume  $V_m$  as  $\gamma_{av} = 3\alpha V_m B_0 / C_v$ . From the microscopic formulation in the quasi-harmonic approximation,  $\gamma_{av}$  can be calculated as  $\gamma_{av} = \sum_i^p C_i \gamma_i / C_v$  where  $p_i$  is the Raman mode degeneracy,  $C_i$  the Einstein molar heat capacity, and  $C_v$  is defined as  $C_v = \sum_i^p C_i$ .<sup>76</sup> In particular,  $C_i$  is obtained as a function of the energy of each mode,  $E_i = h\nu_i$ ,

$$C_i = R \frac{(E_i/k_B T)^2 e^{E_i/k_B T}}{(e^{E_i/k_B T} - 1)^2}, \quad (1)$$

where  $\nu_i$  is the frequency in Hz,  $T$  the temperature, and  $k_B$ ,  $h$ , and  $R$  are the Boltzmann, Planck, and ideal gas constants, respectively.

For the calculation of our experimental and theoretical  $\gamma_i$  in DC-CdGa<sub>2</sub>S<sub>4</sub>, we have used a value of  $B_0 = 40.8\text{ GPa}$  obtained from our *ab initio* simulations under hydrostatic conditions (see Table I); this value is similar to that obtained by Cabrera *et al.* ( $B_0 = 46\text{ GPa}$ ).<sup>28</sup> We have preferred not to use the experimental value ( $B_0 = 64\text{ GPa}$ ) obtained in Ref. 22 because that value was likely overestimated, due to the use of silicone oil as a pressure-transmitting medium. In fact, the value of  $B_0$  for DC and DS compounds under hydrostatic conditions is usually in the range 39–52 GPa.<sup>2,77</sup>

With all these considerations in mind, one can evaluate  $\gamma_i$  for each mode (see Table I). In general, the experimental values of  $\gamma_i$  are found to match quite well with the theoretical values of  $\gamma_i$  obtained from our *ab initio* data. The highest value of  $\gamma_i$  is found for the  $A^1$  mode, ahead of the  $E^3_{TO}$  and  $E^3_{LO}$  modes. The  $B^2_{TO}$  and  $B^2_{LO}$  modes have negative  $\gamma_i$ ; meanwhile, in the rest of the modes  $\gamma_i$  fall between 0 and 1. Our experimental and theoretical  $\gamma_i$  also show a good agreement with the experimental ones of Ref. 26 and with the theoretical ones of Ref. 28, respectively. However, our  $\gamma_i$  do not agree much with those of Ref. 27 because in that work the bulk modulus obtained with the Harrison-Keating model ( $B_0 = 88\text{ GPa}$ ) is more than double than our calculated one. To conclude the discussion of  $\gamma_i$ , only a few other studies dealt with the determination of  $\gamma_i$  in DC and DS-type OVCs, such as ZnGa<sub>2</sub>Se<sub>4</sub> or CdGa<sub>2</sub>Se<sub>4</sub>.<sup>57,78</sup> Taking into account our calculated  $\gamma_i$  and Refs. 57 and 78, we can establish that, in general,  $\gamma_{TO,i} > \gamma_{LO,i}$ . This trend has also been observed in ZB and wurtzite-type  $AX$  and chalcopyrite-type  $ABX_2$  compounds.<sup>45,79–81</sup>

We now turn to calculate  $C_v$ ,  $\gamma_{av}$  and  $\alpha$  from our experimental and theoretical data. For each Raman mode with TO-LO splitting ( $E$  and  $B$ ), we have used a frequency and a Grüneisen parameter obtained from the average between the TO and LO contributions. Besides, for the calculation of  $\alpha$ , an experimental value of  $V_m = 312.44\text{ \AA}^3$ <sup>82</sup> and a theoretical value of  $V_m = 308.99\text{ \AA}^3$  (from our *ab initio* calculations) was used. The temperature,  $T$ , is set to 298 K. Table III summarizes the values of  $C_v$  and  $\alpha$  obtained with our experimental and theoretical data for CdGa<sub>2</sub>S<sub>4</sub>. The values of  $C_v$  and  $\alpha$  measured at 300 K for CdGa<sub>2</sub>S<sub>4</sub> and other DC and DS compounds are also included. We note that our experimental and theoretical results for  $C_v$  are very similar; however, our value for  $C_v$  is 21% smaller than those measured at 300 K in CdGa<sub>2</sub>S<sub>4</sub><sup>83</sup> and in other OVCs.<sup>83,84</sup> On the other hand, we have obtained an average value of the macroscopic Grüneisen parameter,  $\gamma_{av}$ , of 0.46(2) and 0.49(1) from our experimental and theoretical data, respectively.

**TABLE III.** Experimental (exp) and theoretical (the) molar heat capacity,  $C_v$ , and averaged linear expansion coefficient,  $\alpha$ , obtained for CdGa<sub>2</sub>S<sub>4</sub>. Experimental measurements of  $C_v$  and  $\alpha$  in other OVCs are also included for comparison purposes (data from the literature measured at 300 K).

Compound	$C_v$ (J K <sup>-1</sup> mol <sup>-1</sup> )	Compound	$\alpha$ (10 <sup>-6</sup> K <sup>-1</sup> )
CdGa <sub>2</sub> S <sub>4</sub>	130.9 (1) <sup>a</sup> , 131.6 (1) <sup>b</sup> , 162.0 <sup>c</sup>	CdGa <sub>2</sub> S <sub>4</sub>	5.2 (2) <sup>a</sup> , 5.7 (2) <sup>b</sup>
CdIn <sub>2</sub> S <sub>4</sub>	166.8 <sup>c</sup>	CdGa <sub>2</sub> Se <sub>4</sub>	10.97 <sup>c</sup>
ZnGa <sub>2</sub> Se <sub>4</sub>	166.6 <sup>d</sup>	ZnGa <sub>2</sub> Se <sub>4</sub>	2.10 <sup>f</sup>
ZnGa <sub>2</sub> S <sub>4</sub>	164.6 <sup>d</sup>	MnGa <sub>2</sub> S <sub>4</sub>	0.88 <sup>g</sup>

<sup>a</sup>Our experimental data.

<sup>b</sup>Our theoretical data.

<sup>c</sup>Ref. 83.

<sup>d</sup>Ref. 86.

<sup>e</sup>Ref. 87 (obtained in the temperature range 300–873 K).

<sup>f</sup>Ref. 88.

<sup>g</sup>Ref. 84.

These values agree quite well with the typical range of the  $\gamma_{av}$  found in tetrahedral compounds (between 0.5 and 1.25).<sup>71</sup> Regarding the averaged values of  $\alpha$ , they are found between those in other OVCs (see Table III). We note that the positive values of  $\gamma_i$  in most parts of the Raman modes in CdGa<sub>2</sub>S<sub>4</sub> have given a positive value of  $\gamma_{av}$ , which indicates a positive expansion of this DC. This is in agreement with the positive value found in  $\alpha$  for CdGa<sub>2</sub>S<sub>4</sub> and the positive expansion ( $\alpha > 0$ ) found in other DC and DS compounds as shown in Table III. In contrast, in ZrW<sub>2</sub>O<sub>8</sub>, the negative sign of several  $\gamma_i$  at room temperature leads to a negative value for  $\gamma_{av}$  which indicates a negative thermal expansion (NTE). This NTE was found experimentally on ZrW<sub>2</sub>O<sub>8</sub> over a temperature range from 0.3 to 1050 K.<sup>85</sup>

## VI. CONCLUSIONS

We have performed HP-RS measurements in DC-CdGa<sub>2</sub>S<sub>4</sub> up to 25 GPa that have been compared with accurate *ab initio* calculations providing the LO-TO splitting and have allowed us, on the one hand, to assign more clearly the Raman-active modes and, on the other hand, to clarify the previous disagreement between previous HP-RS studies of Ursaki *et al.* and Mitani *et al.* Our measurements show that the ordered DC phase undergoes an irreversible transition to a Raman-inactive structure above 15 GPa, which can be attributed to the DR phase. In contrast to previous HP-RS studies, our RS measurements show evidence of only one stage of disorder above 9 GPa that leads to an intermediate DS phase prior to the PT to the DR phase. On decreasing pressure from 25 GPa, we show that a DZ phase is recovered, whose HP behavior of the Raman modes was studied in a second upstroke. The DZ phase undergoes a reversible PT to the DR phase above 10 GPa. Consequently, this work evidences the irreversibility (reversibility) of the pressure-induced order-disorder (disorder-disorder) DC-to-DR (DZ-to-DR) transition. Finally, we have calculated, both experimentally and theoretically, the microscopic and macroscopic Grüneisen parameters in DC-CdGa<sub>2</sub>S<sub>4</sub> and have estimated both the molar heat

capacity,  $C_v$ , and the average thermal expansion coefficient,  $\alpha$ , for DC-CdGa<sub>2</sub>S<sub>4</sub>. In this sense, the Grüneisen parameter has proven to be a useful tool to give a first approach to evaluate the above-mentioned thermal properties, involving only data from HP experiments.

## ACKNOWLEDGMENTS

The authors thank the financial support of the Spanish Ministerio de Economía y Competitividad (MINECO) under Grant Nos. MAT2016-75586-C4-2/3-P and MAT2015-71070-REDC (MALTA Consolider) and the Generalitat Valenciana under Project No. PROMETEO/2018/123-EFIMAT. E. P.-G., A. M., and P. R.-H. acknowledge computing time provided by Red Española de Supercomputación (RES) and MALTA-Cluster.

## REFERENCES

- 1A. Miller, A. MacKinnon, and D. Weaire, *Solid State Phys.* **36**, 119 (1982).
- 2O. Gomis, D. Santamaría-Pérez, R. Vilaplana, R. Luna, J. A. Sans, F. J. Manjón, D. Errandonea, E. Pérez-González, P. Rodríguez-Hernández, A. Muñoz, I. M. Tiginyanu, and V. V. Ursaki, *J. Alloys Compd.* **583**, 70 (2014).
- 3P. G. Gallardo, *Phys. Status Solidi B* **182**, K67 (1994).
- 4M. L. Cohen, *Phys. Rev. B* **32**, 7988 (1985).
- 5J. W. Kim and Y. J. Kim, *J. Nanosci. Nanotechnol.* **7**, 4065 (2007).
- 6R. Yu, H. M. Noh, B. K. Moon, B. C. Choi, J. H. Jeong, K. Jang, S. S. Yi, and J. K. Jang, *Mater. Res. Bull.* **48**, 2154 (2013).
- 7F. Liang, L. Kang, Z. Lin, Y. Wu, and C. Chen, *Coord. Chem. Rev.* **333**, 57 (2017).
- 8K. N. Ding, W. Jia, and Y. F. Zhang, *Jieyou Huaxue* **32**, 1307 (2013); available at <http://www.cnki.com.cn/Article/CJFDTotaj-JGHX201309006.htm>.
- 9J. Sahariya, P. Kumar, and A. Soni, *Mater. Chem. Phys.* **199**, 257 (2017).
- 10M. M. El-Nahass, E. A. A. El-Shazly, A. M. A. El-Barry, and H. S. S. Omar, *J. Mater. Sci.* **46**, 5743 (2011).
- 11A. M. Salem, *J. Phys. D Appl. Phys.* **36**, 1030 (2003).
- 12I. G. Stamov, N. N. Syrbu, V. I. Parvan, V. V. Zalamai, and I. M. Tiginyanu, *Opt. Commun.* **309**, 205 (2013).
- 13V. N. Kamenshchikov and L. M. Suslikov, *Opt. Spectrosc.* **118**, 614 (2015).
- 14N. N. Syrbu, A. Tiron, V. I. Parvan, V. V. Zalamai, and I. M. Tiginyanu, *Phys. B* **463**, 88 (2015).
- 15R. Vilaplana, O. Gomis, E. Pérez-González, H. Ortiz, F. J. Manjón, P. Rodríguez-Hernández, A. Muñoz, P. Alonso-Gutiérrez, M. Sanjuán, V. V. Ursaki, and I. M. Tiginyanu, *J. Appl. Phys.* **113**, 233501 (2013).
- 16R. Vilaplana, O. Gomis, F. J. Manjón, H. Ortiz, E. Pérez-González, J. López-Solano, P. Rodríguez-Hernández, A. Muñoz, D. Errandonea, V. V. Ursaki, and I. M. Tiginyanu, *J. Phys. Chem. C* **117**, 15773 (2013).
- 17A. Grzechnik, V. V. Ursaki, K. Syassen, I. Loa, I. M. Tiginyanu, and M. Hanfland, *J. Solid State Chem.* **160**, 205 (2001).
- 18O. Gomis, R. Vilaplana, F. J. Manjón, J. Ruiz-Fuertes, E. Pérez-González, J. López-Solano, E. Bandiello, D. Errandonea, A. Segura, P. Rodríguez-Hernández, A. Muñoz, V. V. Ursaki, and I. M. Tiginyanu, *Phys. Status Solidi B* **252**, 2043 (2015).
- 19F. J. Manjón, O. Gomis, P. Rodríguez-Hernández, E. Pérez-González, A. Muñoz, D. Errandonea, J. Ruiz-Fuertes, A. Segura, M. Fuentes-Cabrera, I. M. Tiginyanu, and V. V. Ursaki, *Phys. Rev. B* **81**, 195201 (2010).
- 20O. Gomis, R. Vilaplana, F. J. Manjón, E. Pérez-González, J. López-Solano, P. Rodríguez-Hernández, A. Muñoz, D. Errandonea, J. Ruiz-Fuertes, A. Segura, D. Santamaría-Pérez, I. M. Tiginyanu, and V. V. Ursaki, *J. Appl. Phys.* **111**, 013518 (2012).
- 21R. Vilaplana, M. Robledillo, O. Gomis, J. A. Sans, F. J. Manjón, E. Pérez-González, P. Rodríguez-Hernández, A. Muñoz, I. M. Tiginyanu, and V. V. Ursaki, *J. Appl. Phys.* **113**, 093512 (2013).

- <sup>22</sup>D. Errandonea, R. S. Kumar, F. J. Manjón, V. V. Ursaki, and I. M. Tiginyanu, *J. Appl. Phys.* **104**, 063524 (2008).
- <sup>23</sup>H. A. Rahnamaye Aliabad, H. Vaezi, S. Basirat, and I. Ahmad, *Z. Anorg. Allg. Chem.* **643**, 839 (2017).
- <sup>24</sup>H. A. Rahnamaye Aliabad, S. Basirat, and I. Ahmad, *J. Mater. Sci. Mater. Electron.* **28**, 16476 (2017).
- <sup>25</sup>O. Shikimaka, A. Burlacu, D. Grabco, V. Parvan, C. Pyrtsac, and V. Ursaki, *J. Phys. D Appl. Phys.* **49**, 205302 (2016).
- <sup>26</sup>V. V. Ursaki, I. I. Burlakov, I. M. Tiginyanu, Y. S. Raptis, E. Anastassakis, and A. Anedda, *Phys. Rev. B* **59**, 257 (1999).
- <sup>27</sup>T. Mitani, S. Onari, K. Allakhverdiev, F. Gashimzade, and T. Kerimova, *Phys. Status Solidi B* **223**, 287 (2001).
- <sup>28</sup>M. Fuentes-Cabrera, *J. Phys. Condens. Matter* **13**, 10117 (2001).
- <sup>29</sup>S. Klotz, J. C. Chervin, P. Munsch, and G. L. Marchand, *J. Phys. D Appl. Phys.* **42**, 075413 (2009).
- <sup>30</sup>H. K. Mao, J. A. Xu, and P. M. Bell, *J. Geophys. Res. Solid Earth* **91**, 4673 (1986).
- <sup>31</sup>K. Syassen, *High Press. Res.* **28**, 75 (2008).
- <sup>32</sup>P. E. Blöchl, *Phys. Rev. B* **50**, 17953 (1994).
- <sup>33</sup>G. Kresse and J. Furthmüller, *Phys. Rev. B* **54**, 11169 (1996).
- <sup>34</sup>S. Baroni, S. De Gironcoli, A. Dal Corso, and P. Giannozzi, *Rev. Mod. Phys.* **73**, 515 (2001).
- <sup>35</sup>J. P. Perdew, A. Ruzsinszky, G. I. Csonka, O. A. Vydrov, G. E. Scuseria, L. A. Constantin, X. Zhou, and K. Burke, *Phys. Rev. Lett.* **100**, 136406 (2008).
- <sup>36</sup>J. A. Sans, D. Santamaría-Pérez, C. Popescu, O. Gomis, F. J. Manjón, R. Vilaplana, A. Muñoz, P. Rodríguez-Hernández, V. V. Ursaki, and I. M. Tiginyanu, *J. Phys. Chem. C* **118**, 15363 (2014).
- <sup>37</sup>P. Lottici and C. Razzetti, *J. Mol. Struct.* **115**, 133 (1984).
- <sup>38</sup>T. G. Kerimova, N. A. Abdullaev, I. A. Mamedova, Z. I. Badalova, R. A. Guliev, R. Paucar, K. Wakita, and N. T. Mamedov, *Semiconductors* **47**, 761 (2013).
- <sup>39</sup>I. M. Tiginyanu, P. P. Lottici, C. Razzetti, and S. Gennari, *Jpn. J. Appl. Phys.* **32**, 561 (1993).
- <sup>40</sup>Z. A. Dzhakhangirli, T. G. Kerimova, and N. A. Abdullaev, *Semiconductors* **50**, 285 (2016).
- <sup>41</sup>T. G. Kerimova, I. A. Mamedova, N. A. Abdullayev, S. Q. Asadullayeva, and Z. I. Badalova, *Semiconductors* **48**, 868 (2014).
- <sup>42</sup>C. Razzetti and P. Lottici, *Jpn. J. Appl. Phys.* **32**, 431 (1993).
- <sup>43</sup>I. I. Nebola, L. M. Suslikov, V. S. Dordyai, Y. M. Vysochanskii, N. P. Karkhalis, and V. Y. Slivka, *Fizika Tverdogo Tela* **24**, 3631 (1982).
- <sup>44</sup>N. N. Syrbu, L. L. Nemerenco, and O. Cojocaru, *Cryst. Res. Technol.* **37**, 101 (2002).
- <sup>45</sup>D. Majumdar, A. Basu, G. D. Mukherjee, D. Ercolani, L. Sorba, and A. Singha, *Nanotechnology* **25**, 465704 (2014).
- <sup>46</sup>R. Trommer, H. Müller, M. Cardona, and P. Vogl, *Phys. Rev. B* **21**, 4869 (1980).
- <sup>47</sup>I. Zardo, S. Yazji, C. Marini, E. Uccelli, A. Fontcuberta i Morral, G. Abstreiter, and P. Postorino, *ACS Nano* **6**, 3284 (2012).
- <sup>48</sup>K. Aoki, E. Anastassakis, and M. Cardona, *Phys. Rev. B* **30**, 681 (1984).
- <sup>49</sup>O. Gomis, R. Vilaplana, F. J. Manjón, D. Santamaría-Pérez, D. Errandonea, E. Pérez-González, J. López-Solano, P. Rodríguez-Hernández, A. Muñoz, I. M. Tiginyanu, and V. V. Ursaki, *J. Appl. Phys.* **113**, 073510 (2013).
- <sup>50</sup>O. Gomis, H. M. Ortiz, J. A. Sans, F. J. Manjón, D. Santamaría-Pérez, P. Rodríguez-Hernández, and A. Muñoz, *J. Phys. Chem. Solids* **98**, 198 (2016).
- <sup>51</sup>K. R. Allakhverdiev, *Frontiers of High Pressure Research II: Application of High Pressure to Low-Dimensional Novel Electronic Materials* (Springer, 2001), p. 99.
- <sup>52</sup>P. P. Lottici and C. Razzetti, *Solid State Commun.* **46**, 681 (1983).
- <sup>53</sup>M. L. Sanjuán and M. Morón, *Phys. B* **316**, 565 (2002).
- <sup>54</sup>S. I. Radautsan, I. M. Tiginyanu, V. V. Ursakii, V. M. Fomin, and E. P. Pokatilov, *Phys. Status Solidi B* **162**, K63 (1990).
- <sup>55</sup>J. E. Bernard and A. Zunger, *Phys. Rev. B* **37**, 6835 (1988).
- <sup>56</sup>F. J. Manjón, O. Gomis, R. Vilaplana, J. A. Sans, and H. Ortiz, *Phys. Status Solidi B* **250**, 1496 (2013).
- <sup>57</sup>T. Mitani, T. Naitou, K. Matsuishi, S. Onari, K. Allakhverdiev, F. Gashimzade, and T. Kerimova, *Phys. Status Solidi B* **235**, 321 (2003).
- <sup>58</sup>S. Meenakshi, V. Vijayakumar, B. Godwal, A. Eifler, I. Orgzall, S. Tkachev, and H. Hochheimer, *J. Phys. Chem. Solids* **67**, 1660 (2006).
- <sup>59</sup>F. J. Manjón, B. Mari, J. Serrano, and A. H. Romero, *J. Appl. Phys.* **97**, 053516 (2005).
- <sup>60</sup>A. El Manouni, F. J. Manjón, M. Perales, M. Mollar, B. Mari, M. Lopez, and J. R. Barrado, *Superlattices Microstruct.* **42**, 134 (2007).
- <sup>61</sup>M. I. McMahon and R. J. Nelmes, *Phys. Status Solidi B* **198**, 389 (1996).
- <sup>62</sup>J. M. Binsma, L. J. Giling, and J. Bloem, *Phys. Status Solidi A* **63**, 595 (1981).
- <sup>63</sup>H. Bilz and W. Kress, *Phonon Dispersion Relations in Insulators* (Springer, 1979), p. 110.
- <sup>64</sup>Y. C. Cheng, C. Q. Jin, F. Gao, X. L. Wu, W. Zhong, S. Li, and P. K. Chu, *J. Appl. Phys.* **106**, 123505 (2009).
- <sup>65</sup>M. Güler and E. Güler, *Crystals* **7**, 161 (2017).
- <sup>66</sup>J. Gonzalez, B. J. Fernandez, J. M. Besson, M. Gauthier, and A. Polian, *Phys. Rev. B* **46**, 15092 (1992).
- <sup>67</sup>D. N. Talwar, M. Vandevyver, K. Kunc, and M. Zigone, *Phys. Rev. B* **24**, 741 (1981).
- <sup>68</sup>A. Griesinger, K. Spindler, and E. Hahne, *Int. J. Heat Mass Transf.* **42**, 4363 (1999).
- <sup>69</sup>A. M. Hofmeister and H.-k. Mao, *Proc. Natl. Acad. Sci.* **99**, 559 (2002).
- <sup>70</sup>S. Kasap, P. Capper, and C. Koughia, *Springer Handbook of Electronic and Photonic Materials* (Springer, 2006).
- <sup>71</sup>S. A. Miller, P. Gorai, B. R. Ortiz, A. Goyal, D. Gao, S. A. Barnett, T. O. Mason, G. J. Snyder, Q. Lv, and V. Stevanović, *Chem. Mater.* **29**, 2494 (2017).
- <sup>72</sup>W. G. Zeier, A. Zevalkink, Z. M. Gibbs, G. Hautier, M. G. Kanatzidis, and G. J. Snyder, *Angew. Chem. Int. Ed.* **55**, 6826 (2016).
- <sup>73</sup>T. H. K. Barron, *Ann. Phys.* **1**, 77 (1957).
- <sup>74</sup>A. K. Arora, *J. Phys. Chem. Solids* **51**, 373 (1990).
- <sup>75</sup>E. Grüneisen, *Ann. Phys.* **344**, 257 (1912).
- <sup>76</sup>K. K. Mishra, S. Bevara, T. R. Ravindran, S. J. Patwe, M. K. Gupta, R. Mittal, R. V. Krishnan, S. N. Achary, and A. K. Tyagi, *J. Solid State Chem.* **258**, 845 (2018).
- <sup>77</sup>F. J. Manjón, I. M. Tiginyanu, and V. V. Ursaki, *Pressure-induced Phase Transitions in AB<sub>2</sub>X<sub>4</sub> Chalcogenide Compounds* (Springer, 2014).
- <sup>78</sup>K. Allakhverdiev, F. Gashimzade, T. Kerimova, T. Mitani, T. Naitou, K. Matsuishi, and S. Onari, *J. Phys. Chem. Solids* **64**, 1597 (2003).
- <sup>79</sup>C. Parlak and R. Eryigit, *Phys. Rev. B* **73**, 245217 (2006).
- <sup>80</sup>G. Kern, G. Kresse, and J. Hafner, *Phys. Rev. B* **59**, 8551 (1999).
- <sup>81</sup>B. A. Weinstein and R. Zallen, *Light Scattering in Solids IV* (Springer, 1984), p. 463.
- <sup>82</sup>H. Schwer and V. Krämer, *Z. Kristallogr. Cryst. Mater.* **190**, 103 (1990).
- <sup>83</sup>K. K. Mamedov, M. M. Aliev, and I. G. Kerimov, *Phys. Status Solidi A* **9**, K149 (1972).
- <sup>84</sup>M. Quintero, M. Morocoima, E. Guerrero, and J. Ruiz, *Phys. Status Solidi A* **146**, 587 (1994).
- <sup>85</sup>T. R. Ravindran, A. K. Arora, and T. A. Mary, *Phys. Rev. Lett.* **84**, 3879 (2000).
- <sup>86</sup>K. K. Mamedov, I. G. Kerimov, R. K. Veliev, and M. I. Mekhtiev, *Izvestiya Akademii Nauk SSSR, Neorganicheskie Materialy* **11**, 2062 (1975).
- <sup>87</sup>B. Khuseinov, S. Mavlonov, and B. Umarov, *Inorg. Mater.* **14**, 675 (1978).
- <sup>88</sup>M. Morocoima, M. Quintero, E. Guerrero, R. Tovar, and P. Conflant, *J. Phys. Chem. Solids* **58**, 503 (1997).